

Low speed laser welding of aluminium alloys using single-mode fiber lasers

Jay F. Tu and Alexander G. Paleocrassas
North Carolina State University
USA

1. Introduction

Laser welding of aluminium alloys is an important industrial technology and yet many challenges still lie ahead. Laser welding studies were reported almost within two years since the first laser was invented in 1960. However, practical metal seam welding was not feasible until the early 1970s when multi-kilowatt, continuous wave CO₂ lasers were developed to allow for deep penetration keyhole welding (Duley, 1999). Unfortunately, the application for deep penetration welding of aluminium was limited due to its very high reflectivity at the relatively long wavelength (10.6 micron) of CO₂ lasers. Flash-pumped Nd:YAG lasers with a 1.06 micron wavelength were not suitable due to their low power and extremely poor efficiency at the time. Since the 1980s, high power seam welding of carbon steels using multi-kilowatt CO₂ lasers has become a regular industrial practice, in particular in the automotive industry. In the mid 1990s, diode pumped Nd:YAG lasers were developed that offered kilowatt power and high efficiency. As a result, aluminium laser welding became more feasible because the beam absorption of aluminium alloys at 1.06 micron is three times as much as it is at 10.6 micron. Nevertheless, the poor beam quality and high cost of diode-pumped Nd:YAG lasers still hinders their acceptance in industry. In the early 2000s, with the arrival of single-mode and multi-mode high power fiber lasers at a 1.075 micron wavelength, along with excellent beam quality and low maintenance cost, the expectation was that the advantage of laser welding aluminium components could be better realized.

The requirement of very high laser power for aluminium welding is not only due to its high reflectivity and high heat conductivity. Aluminium has been known to be one of the most challenging metals to weld successfully (Mandal, 2002). Other factors affecting the weld quality of aluminium alloys include different kinds of porosity formation, hot tearing, solidification cracking, oxide inclusions and loss of alloying elements. It has been found that weld porosities can be significantly suppressed at high welding speeds. In order to maintain a stable keyhole at high speeds, very high laser power is needed. What has been less explored is the reason why the welding process becomes less stable and prone to defects as the speed is reduced. There are many applications where high speed welding is not suitable. With the expansion of modern miniaturized consumer products, the weld path can be short and with intricate shapes. High welding speed may not be effective due to the short paths and constant accelerations and decelerations required to follow the path precisely. One such

application is the fusion of fatigue cracks in aluminium parts, where a crack path is irregular. It also has been shown that welding at a lower processing speed can reduce the tendency of transverse solidification cracking. Finally, with the availability of better laser sources such as high power fiber lasers, it is important to expand laser welding of aluminium to wider processing conditions for various applications.

This book chapter will discuss latest research results in extending laser welding of aluminium in the low speed range by investigating the welding instability phenomena. The following topics will be discussed:

- Aluminium alloys and welding defects
- Brief review of high speed laser welding of aluminium
- High power fiber lasers and optical setups
- Process modelling of laser welding of aluminium
- Experimental process characterization of low speed welding
- The instability and defects at low speed welding
- Applications of fatigue crack repair in aluminium

First, the properties of aluminium alloys and the cause of welding defects are discussed. Prior to discussing low speed welding, a brief review of high speed laser welding of aluminium is provided. The characteristics of high power fiber lasers and their optical setups for welding applications, such as focusing lens, assist gas, alignments, and damage prevention due to beam reflection by aluminium are then presented. The chapter then proceeds to present recent research results in low speed laser welding of aluminium, which includes theoretical process modelling, experimental process characterization, in-process monitoring of several critical signals, such as plasma radiation and beam reflection, as well as the causes and consequences of process instability at low speeds. The transition of process stability from medium welding to a low speed threshold and its mechanisms are explored. Finally, an application of low speed laser welding of aluminium for fatigue crack repair is given. A discussion on different applications and future development conclude the chapter.

2. Background and Reviews

2.1 Aluminium Alloys

Aluminium alloys can be separated into two major categories: Non heat-treatable and heat-treatable. The initial strength of non heat-treatable alloys depends primarily upon the hardening effect of alloying elements such as silicon, iron, manganese and magnesium. The non heat-treatable alloys are mainly found in 1xxx, 3xxx, 4xxx and 5xxx series. Additional strength is usually achieved by solid-solution strengthening or strain hardening.

The initial strength of heat-treatable alloys depends upon the alloy composition, just like the non heat-treatable alloys. In order to improve their mechanical properties they need to undergo solution heat treating and quenching followed by either natural or artificial aging (precipitation hardening). This treatment involves maintaining the work piece at an elevated temperature, followed by controlled cooling in order to achieve maximum hardening. The heat-treatable alloys are found primarily in the 2xxx, 6xxx and 7xxx alloy series (ibid).

The 7xxx series alloys contain zinc in amounts between 4 and 8 % and magnesium in amounts between 1 and 3 %. Both have high solid solubility in aluminium. The addition of

magnesium produces a marked increase in precipitation hardening characteristics. Copper additions between 1 and 2 % increase the strength by solid solution hardening, and form the basis of high strength aircraft alloys. The addition of chromium, typically up to 0.3 %, improves stress corrosion cracking resistance. The 7xxx series alloys are predominantly used in aerospace applications, 7075-T6 being the principal high strength aircraft alloy (Ion, 2000). This chapter will focus on fiber laser welding of 7075-T6 because of its predominant use in aircraft components.

2.2 Laser Welding Defects in Aluminium

Laser welding is one of the most promising metal joining methods because it can provide high productivity, high weld quality, high welding speed, high weld aspect ratio, low heat input, low distortion, manufacturing flexibility and ease of automation (Duley, 1999, Mandal, 2002). According to a study on phase transformations in weldments (Cieslak, 1992), solidification rates of 10^2 to 10^3 °C/sec encountered in conventional arc welding processes, are much lower compared to high-energy density laser processes which reach 10^5 to 10^6 °C/sec as a result of high heat input experienced at high travel speeds. Under these processing conditions the weld metal microstructure bears no resemblance to that expected as the result of arc welding. Consequently, the weldment is mostly comprised by fine-grained microstructures.

There are four major types of weld defects in laser welding of aluminium: a) porosity, b) cracking, c) inclusions and d) loss of alloying elements (Matsunawa, 1994, Cao, *et al.*, 2003).

Hydrogen porosity: Hydrogen is very soluble in aluminium and its alloys. Most gas porosities precipitated in aluminium alloys are attributed to hydrogen. The solubility of hydrogen in liquid aluminium is an exponential function of temperature, which is why its porosity is a much bigger problem in laser welding (than in conventional welding) due to increased temperatures. Also, the high cooling rate is very unfavorable because it does not allow for diffusion (i.e. "floatation") of the trapped hydrogen. Normal hydrogen levels in molten aluminium vary from approximately 0.10 to 0.40 mL/100g. It is worth noting here that in order for an aircraft part to pass aerospace quality inspections, the gas contents have to be less than 0.06 mL/100g. A critical lower welding speed possibly exists at which formation and growth of hydrogen porosity can be prevented. Also, another way to reduce hydrogen porosity is to increase power density, because it keeps the keyhole stable and increases solidification time, allowing the hydrogen to escape (Cao, *et al.*, 2003).

According to a study conducted on porosity formation (Kutsuna and Yan, 1998), the rate of hydrogen porosity shows a tendency to rise considerably as the magnesium content increases. This happens because magnesium in aluminium alloys raises the hydrogen solubility in the molten pool and hence the segregation of magnesium enhances the segregation of hydrogen during solidification.

Porosity caused by collapse of unstable keyholes: Even with proper material surface preparation, laser parameters, shielding gas and material compositions, aluminium alloys are susceptible to random porosities after laser welding (Weeter, 1998). Keyhole instability and the coupling of the laser beam into the metal are suspected to cause these random events. These porosities have irregular or turbular form and are large enough to be visible with x-ray analysis (Dausinger, *et al.*, 1997). They are usually located in the keyhole path, whereas hydrogen pores are more or less equally distributed with slight enrichment at the melting line. The number of cavities is strongly influenced by processing parameters such as the

power, focusing and wavelength. Most likely, keyhole stability is increased with the shorter wavelength lasers (Nd:YAG) because the beams are not as drastically affected by the weld plume as the ones with longer wavelength lasers (CO₂). In the latter case, the weld plume periodically blocks the beam from impinging on the metal and thus causes an instability in the keyhole. The shorter wavelength laser beams can pass through the plume and can provide a more consistent heat input into the metal (Weeter, 1998). It has also been observed that the highest level of porosity is concentrated in the regions where an unstable keyhole is formed. They are mainly composed of metal vapor but will condense at room temperature. The way to reduce this type of porosity is to keep the keyhole as stable as possible; this can be achieved by welding at high speeds and the addition of filler wire. Also, the use of high-power continuous wave (CW) can improve the stability of keyholes (Cao, *et al.*, 2003b).

Results based on a study that was conducted in vacuum and under low pressure welding with a tornado nozzle were reported to reduce or suppress porosity. It was also reported that the forward welding with about 15 to 20 degrees of beam inclination was able to reduce porosity (Katayama, *et al.*, 2003). However, full penetration and pulse-modulated welding approaches were not completely effective.

Cracking: Aluminium alloys exhibit a strong propensity for weldment crack formation because of their large solidification temperature range, high coefficient of thermal expansion, and large solidification shrinkage. The restrained contraction of a weld during cooling, sets up tensile stresses in the joint which may cause cracking. There are two types of hot cracking: a) cracking that occurs in the weld fusion zone during solidification of the weld metal which is known as solidification cracking, and b) cracking that takes place in the primary melting zone due to tearing of the liquate, called liquation cracking (Zhao, *et al.*, 1999). These cracks are detrimental to the integrity of the weld since they form areas of high stress concentration and will significantly reduce the strength of the weld, probably leading to catastrophic failure.

Oxide Inclusions: Oxides are one of the main types of inclusions in aluminium alloys. During keyhole laser welding, the inherently unstable keyhole flow may entrap shielding gas or even air because of imperfect gas shielding (Matsunawa, *et al.*, 1998). Additionally, the shielding gas cannot be truly pure; therefore, some oxide particles may be present in the keyhole vapor. The surface of liquid metal in weld pools (strictly speaking, the surface here should be referred to as the interface between the liquid metal in the weld pool and metal vapor or shielding gas) may also be partly oxidized to form oxide films because of the entrapment of air or shielding gas into the pools. Depending on the magnesium contents in aluminium alloys, oxides such as Al₂O₃, Al₂MgO₄, MgO, or their combination may occur. When aluminium alloys contain magnesium, because it is surface active in liquid aluminium, the oxidizing tendency of the molten aluminium increases rapidly with magnesium contents. When the aluminium alloys contain a trace of magnesium, a mixed oxide (MgAl₂O₃), spinel, is formed. When the magnesium content of the alloy exceeds approximately 2%, the liquid oxidizes rapidly to form MgO. The oxides entrained into welded metal because of surface turbulent flow in welding are referred to as young oxides. Oxides in base metal, originally from primary processing of aluminium alloys are termed old oxides.

Loss of Alloying Elements: The high power density used for laser welding may cause selective vaporization of some alloying elements with a low fusion point such as lithium, magnesium, and zinc because of their higher equilibrium vapor pressure than aluminium. Selective

vaporization of alloying elements can take place in both keyhole and conduction mode laser welding. The vaporization mechanism is divided into three stages. The first stage involves transport of vaporization elements from the bulk to the surface of the molten weld pool. Then the vaporization of elements occurs at the liquid/vapor interface, and finally the vaporized species are transported into the surrounding gas phases (Cao, *et al.*, 2003ab). This will also cause a void on the top of the weld called underfill. It was found that the intrinsic vaporization of alloying elements at the weld pool surface, controls the overall vaporization (Zhao, *et al.*, 1999).

The loss of alloying elements can be minimized by controlling the beam power density distribution during continuous wave (CW) laser welding, which can influence the temperature of the molten metal in the welding pool (Cao, *et al.*, 2003ab). Another way of reducing this loss is through the use of filler metal, which is used as an auxiliary source of material to fill the gap. It also provides a means of controlling the metallurgy of the weld bead and ensures weld quality (Ion, *et al.*, 2001), by helping replenish the loss of alloying elements and also prevent solidification cracking. The use of filler metal in laser welding is justified only if the joint gap and sheet metal thickness is larger than the beam and loss of alloying elements is significant (Molian, 2004). Some skepticism remains about the process, mainly because it is considered to be complex and requires high precision. The interactions between the large number of process variables involved are also not fully understood (Ion, *et al.*, 2001).

2.3 High Speed Laser Welding of Aluminium

Dausinger, *et al.*, (1996) reported that with a 2.2 kW Nd:YAG laser, weld depths of up to 3.7 mm in AA 6082 have been obtained at approximately 16.7 mm/s, at a power density of 3 MW/cm². Also, Yoshikawa, *et al.* (1995), report that successful butt welds of 3 mm thick 5 and 6 series aluminium alloys can be obtained. They also used high duty cycle power modulation (pulsing) in order to prevent cracks. In a different study, a 3 kW CO₂ laser has been able to achieve approximately 2.5 mm weld depth in aluminium alloy 7075-T6 at about 25 mm/s (Katayama and Mizutani, 2002). Also, a 4.5 kW CO₂ produced penetration depths of 3.5 mm in aluminium alloy series 5000 (non heat-treatable) and 6000 (heat-treatable), at a speed of approximately 33 mm/s; in comparison, a 4 kW Nd:YAG produced weld depths of 4 mm at the same speed (Cao, *et al.*, 2003a). In addition, Ramasamy and Albright (2000) showed that when welding with a pulsed 2 kW Nd:YAG, or a 3 kW continuous wave Nd:YAG, or a 3-5 kW CO₂ laser, vaporization of magnesium and/or silicon can occur from aluminium alloy 6111-T4 and also the metal hardness was reduced. This means that when operating at very high power densities, loss of alloying elements is a significant problem.

Some other more recent studies are also worth being reviewed. Oi *et al.* (2006) used a slab CO₂ laser for bead-on-plate and filler wire welding of 2.4 mm thick AA 7075-T6. Mechanical properties of these welds were examined and, after heat treatment, achieved tensile strengths between 75 and 84 percent (depending on the filler metal added) of the base metal. Another study on the mechanical properties of laser welded heat-treatable aluminium was conducted by Xu *et al.* (2008). They used a CO₂ laser to weld AA 2519-T87 and examined the weld's microstructure and tensile strength. Results showed that the grains in the welds were very fine and the tensile strength, after heat treatment, reached up to 75 percent of the base metal as compared to 61 percent for MIG welding.

2.4 Single-Mode High Power Fiber Lasers

The power source used in this study is a 300 W, Single-Mode, Ytterbium Fiber Optic Laser. The power unit consists of six 50 W modules which are combined to produce an output power of 300 W. Each module contains a fiber optic bundle through which the laser light resonates. The fiber is doped with a rare earth called ytterbium, and acts as the laser gain medium. Each module contains several diode lasers which serve as the pump (IPG, 2003).

	Fiber Laser	Nd:YAG	CO ₂	Disc
Wall Plug Efficiency	30%	~ 5%	~ 10%	15%
Output Powers	to 50 kW	to 6kW	to 20 kW	to 4 kW
BPP (4/5kW)	< 2.5	25	6	8
Diode Lifetimes	100,000	10,000	N.A.	10,000
Cooling	Air/Water	Dionized	Water	Water
Floor Space (4/5kW)	< 1 m ²	6 m ²	3 m ²	> 4 m ²
Operating Cost/hour	\$21.31	\$38.33	\$24.27	\$35.43
Maintenance	Not Required	Often	Required	Often

Table 1. Characteristics comparisons between major high power industrial lasers (Industrial Laser Solutions, 2005).

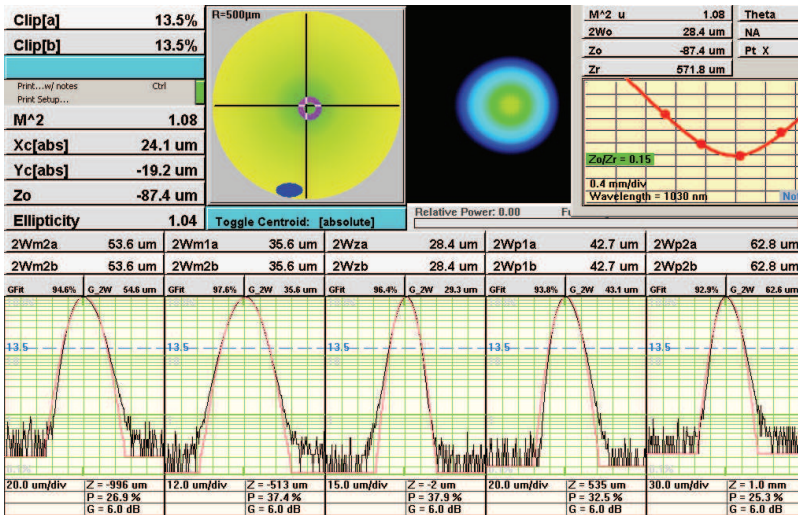


Fig. 1. Beam mode measurement of a 300 W, CW, single-mode fiber laser, provided by IPG, Inc.

A comparison of a high power single-mode fiber laser and other major industrial lasers is listed in Table (1). It is clear that high power fiber lasers have large advantages in wall plug efficiency, maximum output powers, beam quality, reliability and operating cost. Among these advantages, the beam quality, as measured by Beam Parameter Product (BPP) (beam waist radius times divergence angle) and the M² value are most impressive. Their M² value

of approximately 1.08 (Figure 1) is very close to a Gaussian (normal) power distribution. This allows the beam to be focused to a very small spot to achieve very high power densities. In addition to the excellent beam quality, this laser has a wavelength of approximately $1.075\ \mu\text{m}$ (near infrared spectrum), which is relatively short compared to CO_2 lasers. This allows for increased absorption, useful for welding highly reflective materials like aluminium. The beam diameter exiting the collimator is approximately 7 mm, and can be focused down to about $10\ \mu\text{m}$. At 300 W, a maximum power density of about $382\ \text{MW}/\text{cm}^2$ can be achieved.

2.5 Review of Laser Welding with Single-Mode Fiber Lasers

Limited research has been conducted on laser welding using fiber lasers. Prof. Miyamoto was one of the first to realize the advantages of the fiber laser and propose that it be used in laser welding (Miyamoto, et al., 2003). His experiments were performed on stainless steel foil with a limited output power ($\sim 50\ \text{W}$). Ever since, there have been others who have recognized the value of fiber lasers in laser material processing. Allen et al. (2006) used a high power fiber laser as part of a broader study in welding of 7000 series aluminium alloy of thicknesses between 6 and 12 mm. The processing parameters of power and welding speed were not mentioned, however, for proprietary information purposes. Another more recent study (Brown, 2008) focused on keyhole welding on several different metals, including AA 1100, using a moderate power fiber laser (600 W). Uniform high aspect ratio welds were observed, which were in reasonable agreement with the two-dimensional Rosenthal model for a moving-line heat source that was used for comparison. Also, Katayama et al. (2008) used a high power fiber laser to investigate the various welding conditions on penetration and defect formation, on several aluminium alloys and in particular AA5083. Power densities ranged from $40\ \text{kW}/\text{cm}^2$ to $90\ \text{MW}/\text{cm}^2$. At $64\ \text{MW}/\text{cm}^2$ and $10\ \text{m}/\text{min}$ ($166.7\ \text{mm}/\text{s}$) 10 mm thick plates were penetrated fully. Porosity was generated at certain processing conditions, reasons for which were given by interpreting the keyhole and molten metal behaviors, observed using a high speed camera and micro-focused X-ray transmission. It was found that nitrogen gas was more effective than argon, in minimizing or even preventing porosities.

Other research using fiber lasers includes a study on micromachining using a 100 W, single mode fiber laser (Naeem and Lewis, 2006). This research group has focused their study on micro joining and micro cutting various metals using both continuous wave and pulsed modes. Similarly, Wagner (2006) studied high speed micro welding of thin sheets of various metals including aluminium, assessing the potentials for low distortion at high speeds. The processing speeds employed reached $100\ \text{m}/\text{min}$ ($1667\ \text{mm}/\text{s}$).

2.6 Experimental Setup for Fiber Laser Welding

An optical isolator was attached to the collimator and is used to divert any reflected light away from the collimator in order to avoid damage to the fiber due the high reflectivity of aluminium. Consequently, the beam diameter and beam quality were changed slightly. The beam diameter increased from 5 mm in diameter to 7 mm, while the M^2 value goes from 1.08 to 1.15.

A 3x beam expander is used in combination with the 100.1 mm triplet lens to obtain a minimum focus spot size of 12.0 μm . Equation 1 shows how to calculate the minimum spot size.

$$\begin{aligned} \text{Spot size} &= \frac{\text{Lens Focal Length}}{\text{Collimator Optics Focal Length} * \text{Beam Expansion Factor}} * \text{Fiber Diameter} \\ &= \frac{100.1 \text{ mm}}{25 \text{ mm} * 3} * 9 \mu\text{m} = 12.01 \mu\text{m} \end{aligned} \quad (1)$$

The laser beam is centered with respect to the beam expander and the laser head. The laser head contains the focusing triplet and can be adjusted using the outer ring. At the bottom of the cutting head there is a chamber that allows for shielding to flow out through the welding nozzle. This chamber is sealed by a special cover glass and a rubber gasket.

The determination of the laser beam's focusing position was done by using a laser drilling technique. One of the fiber laser's particular characteristics is that when a laser pulse is released, there is an approximately 1,500 W power spike that is output for about 1 μs before it drops to the steady-state power value of 300 W. By pulsing the laser for a very short time, approximately 3 μs , we can take advantage of this power spike and create a very high power density at the focus plane. This enables us to perform laser ablation to form a crater into a stainless steel plate. The focusing technique utilizes this process, by creating spot welds or holes at different z-positions, every 10 μm . A picture is taken of each group of welds/holes and using special calibrated software, the radii are measured and plotted versus the z-focus position.

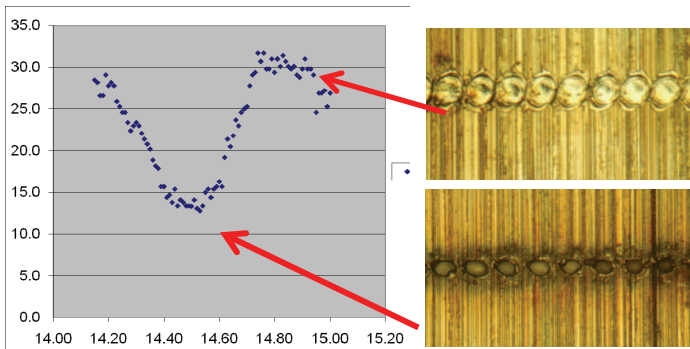


Fig. 2. Spot welds or holes at different focusing locations

Since the laser spot size is very different at different focusing positions, the pulsing will either create very small holes, approximately on the order of the focused beam spot size, or larger spot welds. When all the radii are plotted, the minimum of the resulting curve shows the approximate location of the focusing plane. This is a relatively quick and effective way to find the location of the focus. This technique can be further expanded to obtain the beam profile along its propagation axis (Harp et al, 2008).

3. Low Speed Laser Welding of Aluminium

3.1 Modeling of an Idealized Welding Process

A 2-D heat conduction model for laser welding is reported in Lankalapalli, Tu, and Gartner (1996). This model makes several assumptions which significantly reduce its complexity. The general idea of the model is to calculate the heat conduction over an infinitesimally thin layer of thickness (depth) dz at a specific distance from the top of the surface (Figure 3).

One of the assumptions made, is that the walls of the keyhole within this layer are perpendicular to the surface and that heat conducted in the z -direction is much less than the heat conducted in the radial direction. Therefore, a conical keyhole can be divided into an infinite number of such infinitesimally thin layers and the depth can be approximated by cylindrical heat sources of varying radii, moving together at a constant speed in each of these thin layers. Another assumption made is that there is a quasi-steady state environment in which a cylindrical surface of radius a , at uniform temperature T_v , is moving with a constant speed, v , along the x direction, in an infinite medium initially at constant temperature, T_0 . Finally, assuming that the thermal properties of the medium are constant and that the axis of the cylindrical surface passes through the origin of the coordinate system, the governing differential equations and boundary conditions for the temperature distribution can be written as:

$$\frac{\partial^2 T}{\partial x^2} + \frac{\partial^2 T}{\partial y^2} + \frac{v}{\alpha} \frac{\partial T}{\partial x} = 0 \tag{2}$$

$$T = T_v \text{ at } x^2 + y^2 = a^2 \tag{3}$$

$$T(x, y) \rightarrow T_0 \text{ as } x \rightarrow \pm \infty \text{ and } y \rightarrow \pm \infty \tag{4}$$

where x and y are the surface coordinates, z is the depth coordinate, a is the keyhole radius, v is the welding speed, α is the thermal diffusivity, T_0 is the initial temperature and T_v is the vaporization temperature of the material (Carslaw and Jaeger, 1962).

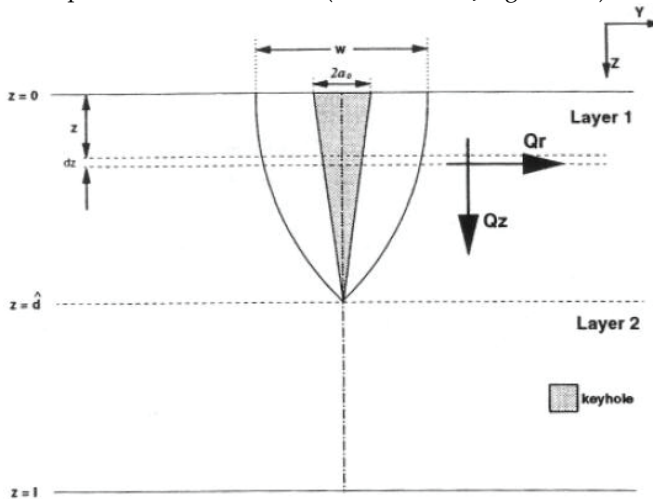


Fig. 3. Keyhole and the resulting weld profile, in which a work piece is sliced to many thin layers (Lankalapalli, Tu, and Gartner, 1996)

After several derivations, the following equation which estimates penetration was found as (Lankalapalli, Tu, and Gartner, 1996)

$$d = \frac{P_i}{k(T_V - T_0)} \frac{1}{\sum_{i=1}^6 \frac{c_i}{i} (Pe_0)^{i-1}} \quad (5)$$

where k is the thermal conductivity of the material and c_i are coefficients to a polynomial fit to the equation that was evaluated numerically for 100 different values of Pe in the operating range of 0 - 0.025:

$$g(Pe) = \int_0^{2\pi} G(\theta, Pe) d\theta = C_1 + C_2 Pe + C_3 Pe^2 + C_4 Pe^3 + C_5 Pe^4 + C_6 Pe^5 \quad (6)$$

where

$$G(\theta, Pe) = Pe * e^{(Pe \cos \theta)} * \sum_{n=0}^{\infty} \varepsilon_n I_n(Pe) \cos(n\theta) \frac{n}{Pe} \frac{K_{n+1}(Pe)}{K_n(Pe)} \cos \theta \quad (7)$$

$$= \frac{T_V - T}{r^*} \frac{T_V - T}{T_V - T_0} \Big|_{r^*=1}$$

$$\frac{T_V - T}{T_V - T_0} = 1 - e^{(-Pe * r^* \cos \theta)} * \sum_{n=0}^{\infty} \varepsilon_n \frac{I_n(Pe)}{K_n(Pe)} K_n(Pe * r^*) \cos(n\theta) \quad (8)$$

is the closed-form solution in polar coordinates (r, θ) of the aforementioned governing differential equation with the specified boundary conditions for the temperature distribution, where $Pe = v^* a / (2\alpha)$ is the Péclet number, $r^* = r/a$ is the normalized radial coordinate, $\varepsilon_n = 1$ for $n = 0$ and 2 for $n \geq 1$, I_n is a modified Bessel function of the first kind, of order n and K_n is a modified Bessel function of the second kind of order n . Note that the above model is not material specific. With proper material parameters and process parameters incorporated, this model allows for very rapid simulation of the temperature field at the top surface (Equation 8) and for an estimation of penetration depth (Equation 5). This model has been validated over a wide range of speed and laser power, different materials, and different lasers (Lankalapalli, Tu, and Gartner, 1996; Paleocrassas and Tu, 2007), as shown in the next section.

3.2 Model Validation through High Speed Welding of SUS 304

Several SUS 304 specimens, 300 microns thick, were welded at relatively high speeds (200–1000 mm/s) (Miyamoto, *et al.*, 2003). In order to determine the operating Péclet number, apart from the welding speed and the thermal diffusivity, the keyhole radius is also required. Determining the keyhole radius is not trivial. There exists a method (Lankalapalli, Tu, and Gartner, 1996) to estimate the Péclet number from the weld width. The idea is that a contour plot of isotherms can be generated for specific Péclet numbers for the top surface using Equation 8, and by measuring the width of the curve corresponding to the melting temperature range, the normalized weld width (w/a) and Péclet number can be correlated.

The normalized weld width is obtained by taking twice the maximum y value (due to symmetry) of the melting temperature isotherm curve. Therefore, an equation can be calculated numerically which can be used to determine the Péclet number at the surface of the specimen, for a corresponding weld width.

Figure 4 shows the model prediction compared to the experimental results from Miyamoto et al (2003). The model predicts a satisfactory trend of penetration change versus the Péclet number for different laser powers. However, the data of a specific laser power usually match the predictions of a lower laser power. For example, the data of 170 W laser power match the predictions of 130 W laser power, data of 130 W match better with prediction at 90 W, etc. Based on this observation, it can be stated that approximately 70-80% of laser power is absorbed. This absorption is relatively low, likely due to the very high welding speed.

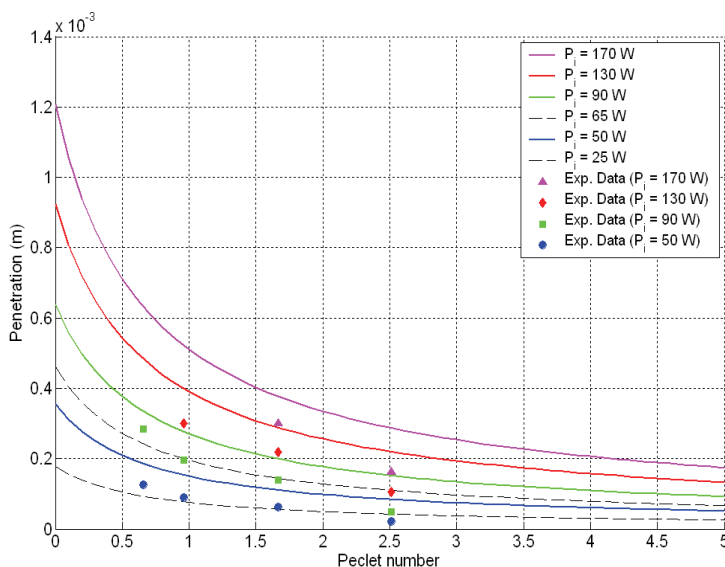


Fig. 4. Theoretical estimate vs. experimentally measured penetration depth in SUS 304.

3.3 Model validation using low speed welding of AA 7075-T6

Figure 5 presents the data/simulation comparison based on the same model for low speed welding of AA7075-T6. As in Figure 4, the model predicts a satisfactory trend of penetration versus the Péclet number. The laser beam absorption is about 90% for welding speeds from 2 mm/s to 10 mm/s. Note that Figures 4 and 5 cover a wide range of Péclet numbers (from 0.5 to 2.5 in Figure 4 and 0.001 to 0.08 in Figure 5). The absorption in Figure 5 is higher than those in Figure 4, likely due to slower welding speed and deeper penetration even though stainless steel is used in Figure 4, while aluminium is used in Figure 5. Once keyhole is formed, the laser beam is absorbed efficiently. For those conditions in Figure 4 with very high welding speeds, the keyhole is shallower and likely tilted to reflect beam power (Fabbro and Chouf, 2000).

However, the point corresponding to 1 mm/s shows a significant decrease in penetration, with its absorbed power being only 68% of the input power. Also, by observing the cross-

sections of the welds at three different processing speeds, it can be seen that the 1 mm/s weld is significantly different from the other two. The 1 mm/s weld shows a significant decrease in aspect ratio. In some cross-sections, large blowholes and porosities were present. The other two welds show more of a conical shaped cross-section, a higher aspect ratio and the absence of any major defects.

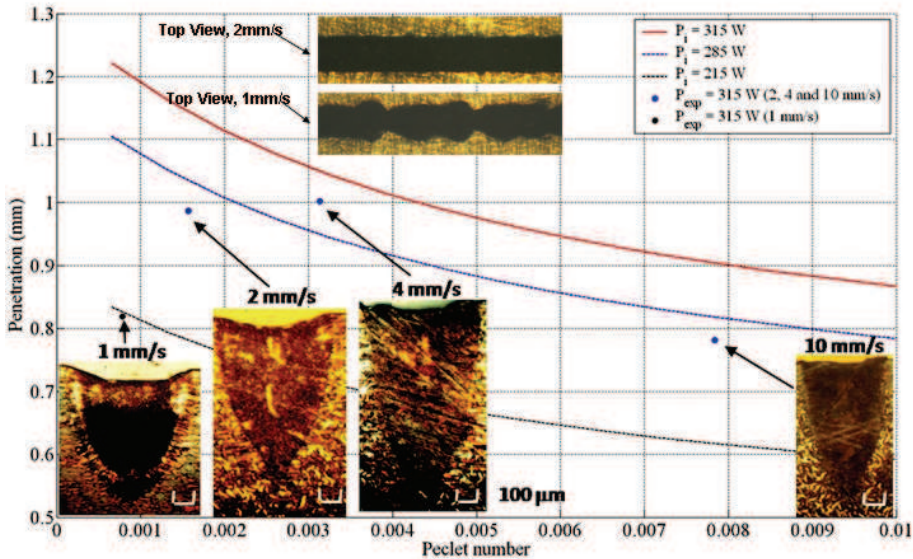


Fig. 5. Model validation for low speed welding of AA 7075-T6

This observation leads to the suspicion that at extremely low speeds the process breaks down and the laser energy is not coupled as efficiently. If this is the case, the model no longer applies to speeds below 2 mm/s.

3.4 Effect of Focusing Positions on Low Speed Welding

Figure 6 shows the change in weld penetration as the focusing position changes (positive indicating the beam is focused into the workpiece).

The general trend is that the best focus position corresponds with the maximum weld depth. This goes along with the recommendation for most welding processes, which is that the focus should be positioned at the desired weld depth (Steen, 2003). Another observation that can be made is that, as the beam is focused past the maximum depth location, the penetration drops at a much higher rate, with the exception of the 10 mm/s condition. This is an indication that the slower speeds are much more sensitive to focusing changes, which means that higher focusing is required to produce adequate and repeatable weld penetrations.

Specifically, for the 10 mm/s processing speed, the maximum weld penetration is approximately both ~ 0.8 mm and this occurs when the focus is approximately 0.9 mm into the workpiece. For the 2 and 4 mm/s speeds the weld penetration is deepest (~ 1 mm) when

the beam is focused approximately 1 mm into the workpiece. The difference in weld penetration (~ 0.8 mm) between these two speeds is not much, with the 4 mm/s weld being slightly deeper. However, the 1 mm/s welds show a significant drop in penetration.

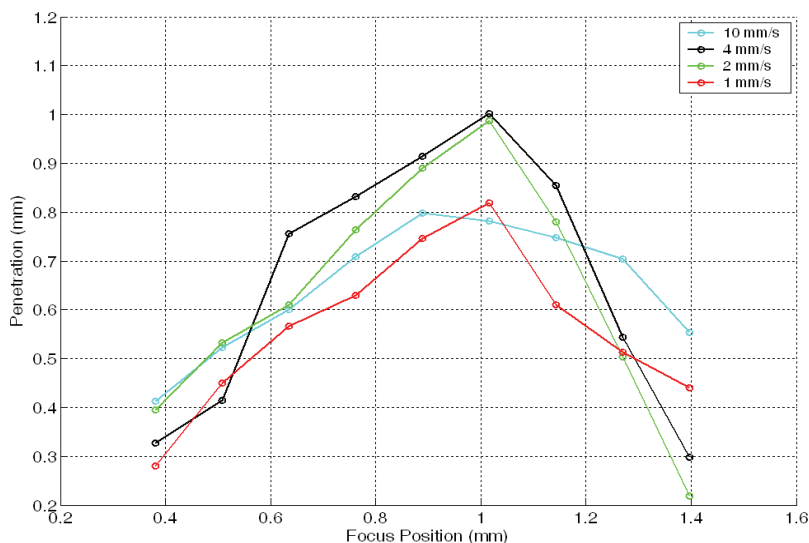


Fig. 6. Effects of focusing position on penetration for different welding speeds.

3.5 Energy-Based Process Characterization

Paleocrassas and Tu (2007) proposed metrics to characterize welding process efficiency. One such metric was defined as keyhole fluence per weld length (KF) which has since been slightly modified and is redefined as follows:

$$KF = \frac{P_i}{A_b} \cdot \frac{l_w}{v} \cdot \frac{1}{l_w} = \frac{P_i}{A_b \cdot v} \quad (9)$$

where P_i is total incident power, A_b is the outer surface area of the immersed laser beam (as calculated from the beam profile approximation, also shown in Figure 8.7), l_w is the length of the weld and v is the processing velocity. This metric represents the total irradiated energy density per weld length.

As mentioned before, due to different types of power losses during welding, the total irradiated energy density per weld length (KF) from the laser is not going to be completely absorbed by the material. Therefore it is of interest to determine the “weld efficiency” by looking at the total energy used to create the weld and how “well” it is used; for example, the same amount of absorbed weld energy could translate into a shallow and wide weld, or a deep and narrow weld.

Specific weld energy per weld length was also defined by Equation 10 to define how well the amount of energy that used to created the weld was used. In this paper, this metric is denoted as Effective Weld Energy (EWE):

$$EWE = \frac{m_{weld} \cdot \zeta}{\pi \cdot r_{profile}^2} = \frac{\rho \cdot V_{weld} \cdot \zeta}{\pi \cdot r_{profile}^2} = \frac{\rho \cdot A_{weld} \cdot \zeta}{\pi \cdot r_{profile}^2} \quad (10)$$

where m_{weld} , V_{weld} , A_{weld} , and $r_{profile}$ are the mass, volume and radius of the top profile (or half of the weld width) of the weld (Figure 7), respectively, ρ is the density and ζ is the specific energy of AA 7075-T6, which is determined by

$$\zeta = C_p \cdot \Delta T + \text{Latent Heat of Fusion} \quad (11)$$

where C_p is the specific heat capacity and ΔT is the temperature change between ambient temperature and the melting point.

Figure 8 was generated by applying the above energy based process characterization to the experimental data. The EWE of each data point is plotted with respect to the input KF. There are four sets of data and each set is connected by a different colored line, corresponding to a different processing speed. The 1, 2, 4 and 10 mm/s data are shown in red, green, black and cyan, respectively. Each data point in each set corresponds to a weld created with a different focusing position. The number next to each data point represents how deep the beam is focused into the workpiece, in thousands of an inch. The first observation that can be made is that for each processing speed, the point that has the highest EWE is the one where the beam was focused at approximately 1 mm (.040 in.) into the workpiece, which indicates that it is the focusing condition that produces the best energy coupling. This is the case because the majority of the vapor pressure used to maintain a certain depth is created at the bottom of the keyhole.

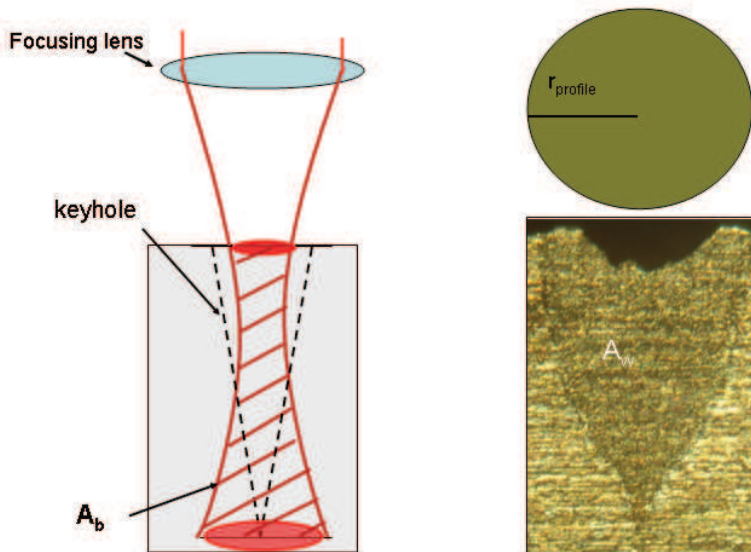


Fig. 7. Schematics showing the submerged beam surface area (A_b), the weld's cross-sectional area (A_w) and the profile radius ($r_{profile}$)

Therefore, placing the focus at the desired weld depth ensures that the maximum power density will be at the bottom of the keyhole, creating the majority of the metal vapor. However, focusing too deep can have an adverse effect on EWE because a minimum power density at the surface is required to create and maintain vaporization of the metal. This explains why the EWE decreases when the laser beam is focused too deep.

By examining the processing speed trend, it was observed that as the speed decreases, the EWE increases, until the speed drops below 2 mm/s. It can therefore be seen that the process is not only dependent on the amount of KF, but also in the manner it is deposited into the workpiece. This leads to the examination of the efficiency of the process.

Global Efficiency: One of the primary concerns in any process involving energy exchange is how efficient it is; in this case, that is, how much of the irradiated energy density per weld length was translated into a desirable, high aspect ratio weld. This is where we can define the “global efficiency” of the process. It is simply the ratio between EWE and KF, as stated in Equation 12.

$$\text{Global Efficiency} = \frac{EWE}{KF} \tag{12}$$

With this metric, we can determine the efficiency at each speed and at each focusing position. If we look at the actual percentages, we will see that the highest efficiency does not exceed 3 percent of the total KF. This might seem extremely low at first, but it is important to remember that this number corresponds only to the energy used to create the weld itself.

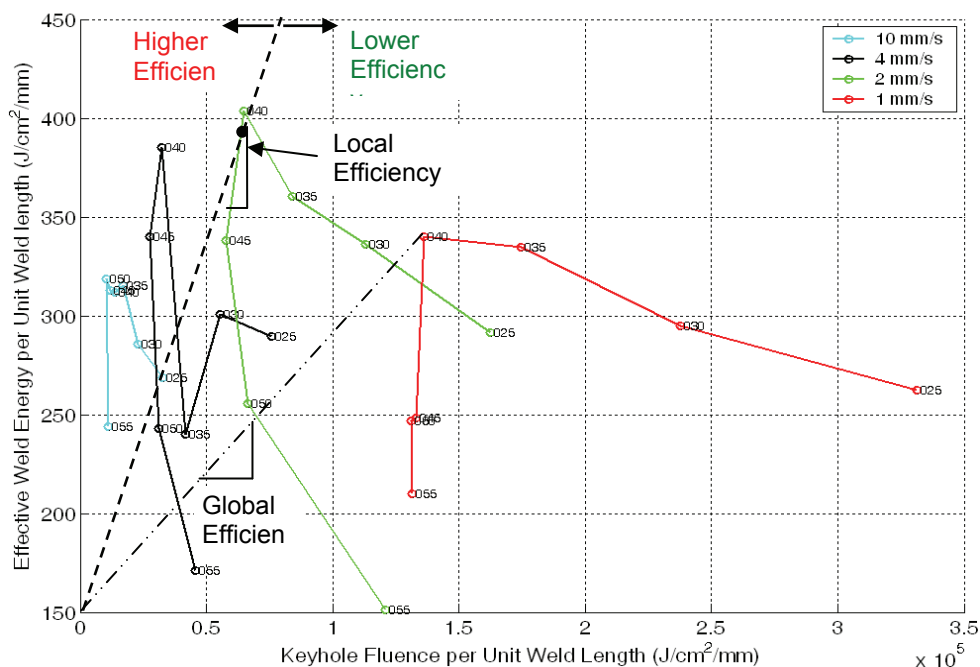


Fig. 8. Variation of effective weld energy with respect to keyhole fluence

During the process, a substantial portion of the absorbed power is conducted away. Therefore the relative change in global efficiency is of more interest than the actual number itself. Looking at the four speeds we observe that the global efficiency decreases slightly from the 10 mm/s data to the 4 mm/s and then slightly lower to 2 mm/s, but drops significantly at the 1 mm/s data. This is another indication that even though there is an increase in KF, the energy is not used as effectively to create a deep and narrow weld. This phenomenon, i.e. the process breakdown of laser welding at extremely low speeds, requires further investigation to explain the reasons behind this drastic change.

Local Efficiency: Another metric we can define to measure the efficiency between different focusing points for a specific processing speed is the "local efficiency." The slopes of these lines can be defined as a "local efficiency" which signifies how efficient the process is, as the focusing changes and the KF increases. In other words it is the ratio of the change in EWE and the change in KF for a particular processing speed (Equation 13).

$$\text{Local Efficiency} = \frac{dEWE}{dKF} \quad (13)$$

It is apparent that the local efficiency is only positive between the weld with the best focusing position and the one that is focused slightly deeper. Again, this is evidence that increasing the KF is not enough to create a good weld, it has to be deposited correctly. It seems that this happens because, when the beam is focused too deep, the incident power density at the surface of the workpiece is not sufficient to create enough vaporization to sustain a keyhole. The process, therefore, switches to conduction welding mode, where a weld is created solely from melting, resulting in a shallow and wide weld. Conversely, if the focus is too close to the surface of the workpiece, the process is again inefficient because the power density at the bottom of the keyhole is too low and cannot sustain the vaporization required for a deeper keyhole.

4. Inherent Process Instability

Table (2) lists the EWEs, global efficiencies, and power efficiencies for the data shown in Figure (8). They clearly showed that the welding became less efficient (from 2.25 % to 0.25 % as the speed drops from 10 mm/s to 1 mm/s) and the quality and aspect ratio of the weld started deteriorating after the processing speed was decreased below 2 mm/s. Large porosities were observed in these very low speed welds in aluminium. This phenomenon is denoted as inherent process instability. In the following sections, the potential contributors of this instability are examined.

Speed (mm/s)	EWE (J/mm ³)	Power Efficiency	"Global" Efficiency
10	312.0	~ 90 %	~ 2.25 %
4	385.0	~ 90 %	~ 1.19 %
2	403.4	~ 90 %	~ 0.62 %
1	340.0	~ 68 %	~ 0.25 %

Table 2. Decrease in EWE and efficiency when speed drops to 1 mm/s.

4.1 Laser Power Distribution

Assuming the laser welding process reaches a quasi-steady state condition, the power distribution, rather than energy distribution, is used to break down the laser power into several components:

$$P_{in} = P_{weld} + P_{cond} + P_{evap} + P_{ref} + (1 - \alpha) \cdot P_{vap/plasma} + P_{scat} \quad (14)$$

where P_{in} is the input power from the laser radiation, P_{weld} is the power used to form the weld similar to the definition of EWE, P_{cond} is the power absorbed by the workpiece and then conducted away into the bulk material, P_{evap} is the power absorbed to produce vapor/plasma, P_{ref} is the power reflected away by the workpiece, $P_{vap/plasma}$ is the power absorbed by the vapor/plasma plume hovering above the workpiece, P_{scat} is the power which is scattered away by the vapor/plasma, and α is the fraction of the power absorbed by the vapor/plasma that is re-radiated on the workpiece and absorbed by the workpiece.

All six terms on the right hand side of Equation 14 are unknown. No attempt is made to solve this equation or to measure each of these unknowns precisely. Dividing both sides by P_{in} , Equation 14 becomes

$$I = \frac{P_{weld}}{P_{in}} + \frac{P_{cond}}{P_{in}} + \frac{P_{evap}}{P_{in}} + \frac{P_{ref}}{P_{in}} + \frac{(1 - \alpha) P_{vap/plasma}}{P_{in}} + \frac{P_{scat}}{P_{in}} \quad (15)$$

Each term on the right-hand side of Equation 15 represents the respective percentage of the laser input power. Based on Table (2), it has been confirmed that P_{weld} / P_{in} drops significantly, which should result in changes in some of the rest of the five terms. Therefore, instead of determining the precise value of each term in Equation 15, the attempt is made to determine how the rest of the five terms change as the welding speed drops from 10 mm/s to 1 mm/s.

4.2 Laser Beam Reflectivity Measurements

Among those losses in Equation 14, we first investigate the reflective loss, P_{ref} , to determine if it is a major factor to cause process instability.

Figure (9) shows the reflected laser beam measured by a photodiode at different welding speeds. For each test, the laser beam is first irradiated at the target, remaining stationary for 5 seconds, before actual welding started at speeds from 10 mm/s to 1 mm/s. In every plot, during this 5 second duration in the beginning of the process, there is a large, sudden increase in intensity which gradually dies off to almost a zero state. The substantial reflected laser radiation in the beginning is due to the beam being reflected by the flat surface of the workpiece. As a keyhole forms, the laser beam penetrates deeper into the workpiece and eventually is absorbed by multiple reflections by the keyhole wall. As a deep keyhole acts like a black body, trapping nearly 100 percent of the laser beam, no reflected laser radiation is detected after about 2 seconds, when the keyhole becomes deep enough. After 5 seconds have passed, the workpiece is then translated at the specified welding speed.

When the workpiece begins to move, the reflected signal appears, again, as a series of high frequency spikes, but with a low average intensity, between 0.25 and 0.4 (a.u.). This is pretty

Thank You for previewing this eBook

You can read the full version of this eBook in different formats:

- HTML (Free /Available to everyone)
- PDF / TXT (Available to V.I.P. members. Free Standard members can access up to 5 PDF/TXT eBooks per month each month)
- Epub & Mobipocket (Exclusive to V.I.P. members)

To download this full book, simply select the format you desire below

